Biophysical *Journal*
Article

Biophysical Society

Mechanical Properties of a *Drosophila* Larval Chordotonal Organ

Achintya Prahlad,[1] Christian Spalthoff,[2] Deqing Kong,[3] Jörg Großhans,[3] Martin C. Göpfert,[2] and Christoph F. Schmidt[1,*]

[1]Faculty of Physics and [2]Faculty of Biology, University of Göttingen, Göttingen, Germany; and [3]Institute of Developmental Biochemistry, University Medical Centre, Göttingen, Germany

ABSTRACT Proprioception is an integral part of the feedback circuit that is essential for locomotion control in all animals. Chordotonal organs perform proprioceptive and other mechanosensory functions in insects and crustaceans. The mechanical properties of these organs are believed to be adapted to the sensory functions, but had not been probed directly. We measured mechanical properties of a particular chordotonal organ—the lateral pentascolopidial (lch5) organ of *Drosophila* larvae—which plays a key role in proprioceptive locomotion control. We applied tension to the whole organ in situ by transverse deflection. Upon release of force, the organ displayed overdamped relaxation with two widely separated time constants, tens of milliseconds and seconds, respectively. When the muscles covering the lch5 organ were excised, the slow relaxation was absent, and the fast relaxation became faster. Interestingly, most of the strain in the stretched organ is localized in the cap cells, which account for two-thirds of the length of the entire organ, and could be stretched by ~10% without apparent damage. In laser ablation experiments we found that cap cells retracted by ~100 μm after being severed from the neurons, indicating considerable steady-state stress and strain in these cells. Given the fact that actin as well as myosin motors are abundant in cap cells, the results point to a mechanical regulatory role of the cap cells in the lch5 organ.

INTRODUCTION

Animal locomotion involves a close interaction between muscles and mechanosensory feedback elements—the proprioceptive organs. Mechanosensory organs are expected to be adapted to the specific motion patterns they need to detect (1). The crawling of *Drosophila* larvae is a relatively simple type of locomotion, involving periodic contractions that travel along the larval body (2). Proprioception in crustaceans and insects is performed by chordotonal organs (3) that are typically serially arranged along the body to monitor relative movements between body parts during locomotion. Chordotonal organs are furthermore involved in detecting substrate vibrations, sound, gravity, and wind (3–8). Anatomically, chordotonal organs consist of one or several multicellular units named "scolopidia". Each scolopidium consists of one to three mechanosensory neurons and several supporting cells. The neurons are bipolar, bearing a proximal axon and a distal dendrite whose outer segment terminates in a cilium. The cilia of all the neurons of each scolopidium are immersed in endolymph that is enclosed by a supporting scolopale cell. The scolopale cells also contain an intracellular barrel of actin-based rods, the scolopale, that surrounds the cilium. The neurons are spanned proximally and apically between opposing cuticular regions by a ligament and a cap cell, respectively. The connections with the cuticle are made by attachment cells (3,9–11).

Development, physiology, and genetics of chordotonal organs have been studied (4,12–17), yet little is known about their intrinsic biomechanics and the molecular mechanisms of mechanosensing. This holds true in general for mechanosensory processes in animals all the way from bacteria to mammals (18). There is consensus, nevertheless, that ion channels in the cell membrane, including, e.g., certain TRP family members, are directly opened by the forces to be measured, which leads to the electrical depolarization of the sensory neuron (19–21). Similar to what was first found for mammalian hair cells in the inner ear (22–26), work on *Drosophila* antennae has shown that antennal chordotonal organs are mechanically active, and nonlinearly boost mechanical input. This capability was linked to the interplay between mechanosensory membrane channels and ciliary dynein motors (13,14,27,28). These findings were based on indirect measurements of antennal mechanics. Direct mechanical measurements on *Drosophila*

Submitted March 8, 2017, and accepted for publication August 7, 2017.
*Correspondence: christoph.schmidt@phys.uni-goettingen.de
Editor: Jennifer Ross.
https://doi.org/10.1016/j.bpj.2017.08.061
© 2017 Biophysical Society.

CrossMark

chordotonal organs have, to the best of our knowledge, hitherto not been reported. Field and Matheson (3) mentioned unpublished data indicating that the elastic properties of a locust chordotonal organ obey Hooke's law. Quantitative measurements of the strain compliance were reported for the femoral chordotonal organ of a stick insect (29), and the impact of length changes on chordotonal organ tension had been measured in a crayfish (30).

Here we report on the mechanics of the lateral pentameric chordotonal organ (lch5), a major chordotonal organ in *Drosophila* larvae (Fig. 1). The lch5 organ occurs bilaterally in the abdominal segments, where it functions in proprioception (31) and possibly also in the detection of sound-induced substrate vibrations (32). Each lch5 organ is suspended between two points on the cuticle at an oblique angle in the dorsal part of the segment and contains five scolopidia with one mechanosensory neuron each. We used a fillet preparation (33) of third instar larvae and explored the mechanical response of the organs by direct deflection. We present data on lch5 shape distortion that reflects elastic embedding, relaxation kinetics that reflect viscous damping, and elastic recoil upon targeted laser ablations that reflects the steady-state elastic strain in the organ. In addition to providing, to our knowledge, first insights into lch5 mechanics, our results highlight the role of the cap cells in setting—and presumably regulating—chordotonal organ tension.

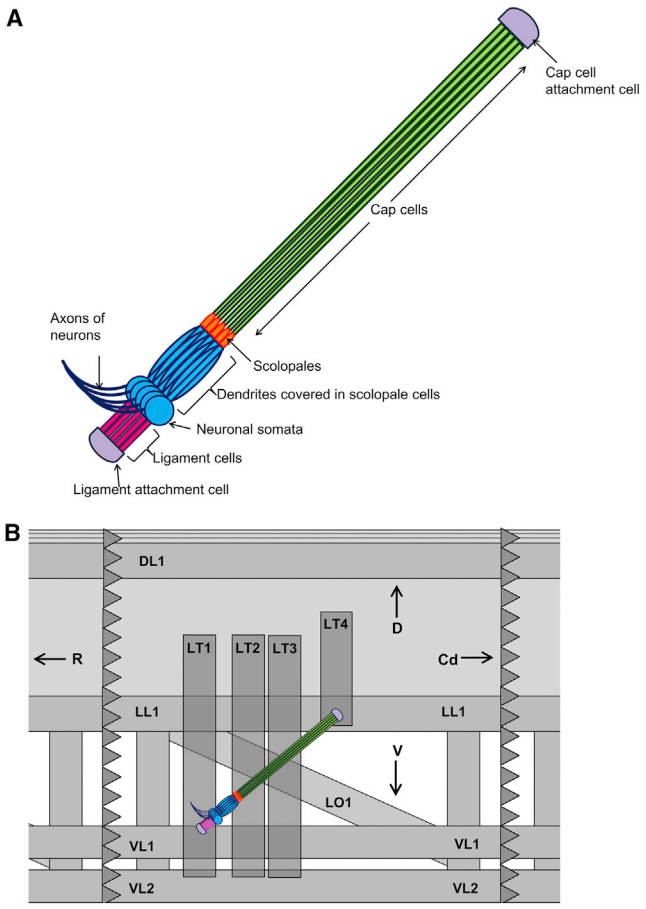

FIGURE 1 Schematic of the lch5 organ of the *Drosophila* larva (10,11). (*A*) Components of the organ. (*B*) Lateral view of a right hemisegment of the larva, oriented such that the rostral end, R, of the larva is to the left and the caudal end, Cd, is to the right. Dorsal direction is D; ventral direction is V. Gray rectangles indicate the muscles that overlay the lch5 organ toward the inside of the larva. The dorsal longitudinal muscle is DL1; lateral transverse muscles are LT1–4; lateral longitudinal muscle is LL1; lateral oblique muscle is LO1; and ventral longitudinal muscles are VL1 and VL2 (there are three more VL muscles, as well as more oblique and LL muscles, which are not shown here). To see this figure in color, go online.

MATERIALS AND METHODS

Relaxation dynamics

Preparation and dissection of Drosophila larvae. We used third-instar Canton-S (http://flybase.org/reports/FBsn0000274.html) wild-type larvae for all experiments and essentially followed published procedures (33). Dissection was carried out on circular PDMS slabs of 30 mm diameter and ~4 mm edge height with a shallow central depression of ~2 mm, which were prepared as described below. The slab was placed in a plastic petri dish of 10 cm diameter. For dissection we used DuMont No. 55 Forceps and Ultra-Fine Clipper Scissors (Fine Science Tools, Heidelberg, Germany). Larvae were dissected under Ringer's solution using a stereomicroscope (model No. M80; Leica Microsystems, Wetzlar, Germany) at 2.5× magnification, and the gut was completely removed using forceps. The larva was then fully opened out and pinned flat. The pins were pieces of 0.1-mm-diameter steel wire. The preparation (fillet) was washed two to three times using Ringer's solution. The larvae were then kept under fresh Ringer's solution and used in the experiments within 10 min after beginning the preparation, and for not longer than 2 h.

In some preparations, we additionally excised muscles using Vannas Spring Scissors (Fine Science Tools). This was done to expose the lch5 organs and compare the relaxation properties to the case where the muscles were intact. The same stereomicroscope was used, and the excision was done at 6× magnification.

To prepare Ringer's solution, the following ingredients were dissolved in high-purity Milli-Q water (Millipore, Billerica, MA): NaCl 0.07 M (Merck, Darmstadt, Germany), KCl 5 mM (Carl Roth, Karlsruhe, Germany), $NaHCO_3$ 0.1 M (Honeywell Riedel de Haën, Seelze, Germany), trehalose 5 mM (Sigma-Aldrich, Munich, Germany), sucrose 0.115 M (AppliChem, Omaha, NE), $CaCl_2$ 2 mM (Carl Roth), $MgCl_2$ 0.02 M (Carl Roth), and HEPES 4.2 mM (Carl Roth). The pH was adjusted to 7.2. Ringer's solution was stored frozen and thawed before use.

Preparation of PDMS slabs (34). Elastomer and curing agent (Sylgard 184 Silicone Elastomer Kit; Dow Corning, Wiesbaden, Germany) were thoroughly mixed at a ratio of 10:1 (4 mL elastomer, 0.4 mL curing agent) in a borosilicate glass beaker of 30 mm inner diameter and baked for 10 min in an oven preheated to 150°C, followed by freezing at −20°C for 5 min to help detach the PDMS from the beaker walls. Through adhesion to the beaker walls before polymerization, the PDMS slabs developed slightly elevated edges that helped retain the buffer solution under the microscope. The slabs were carefully extricated from the beakers using a scalpel.

Preparation of tungsten needles. Tungsten wire (0.2 mm diameter) was purchased from Goodfellow, Bad Nauheim, Germany. Fine-tipped tungsten needles were produced by electrolytically sharpening pieces of this wire on a custom-built machine. The sharpening was carried out by repeatedly dipping the wire into concentrated KOH solution (2 M) using a rotary mechanism. The tip of the needle was bent at an angle of ~90° for a length of ~2 mm, so that it could be hooked into the lch5 organ vertically.

Imaging and mechanical manipulation. The fillet preparation was viewed using a 20× water-dipping objective (W Plan-Apochromat 20×/NA 1.0;

Carl Zeiss Microscopy, Göttingen, Germany) in a custom-built upright microscope equipped with a high-speed camera (Photron Fastcam; VKT Video Kommunikation, Pfullingen, Germany). Using a micromanipulator (Scientifica UI-1000-i; Multichannel Systems, Reutlingen, Germany), the tungsten needle was brought in at an angle of 90° to the lch5 organ. The needle was placed in contact with the cap cells, close to the scolopales, which are a conspicuous feature of the lch5 organ and can be resolved at an accuracy of ~1 μm. A lateral pushing or pulling force was then exerted to deform and stretch the lch5 organ (Movie S4). The displacement amplitude ranged from 20 to 100 μm, and could be measured to an accuracy of 1–2 μm with the objective and camera used. The needle was then rapidly disengaged from the cap cells using the Step function of the manipulator. Videos were recorded at frame rates of 250 and 1000 fps. For the larval preparations with intact muscles, a recording rate of 250 fps was sufficient to resolve the fast time constant of relaxation. For the preparations with muscles excised, a frame rate of 1000 fps was used, because the initial relaxation was faster than in the previous case (Results and Discussion). The videos were analyzed using the Manual Tracking plugin of the software ImageJ (https://imagej.nih.gov/ij/plugins/track/track.html) by specifically tracking the motion of the distinctive scolopales. In the preparations with intact muscles, four lch5 organs, each from a different animal, were tested (two, six, five, and five trials, respectively). For the case with excised muscles, three trials each were performed on two organs from two different animals. The position data obtained from ImageJ was fitted by single or double exponentials in the software OriginPro (http://www.originlab.com/Origin). To directly compare both relaxation dynamics, we also determined the times needed for the relaxation of the amplitudes to 50% from the fit functions using the software MATLAB (The MathWorks, Natick, MA).

Further videos were recorded at 20 fps, using a charge-coupled device camera (Photometrics Coolsnap EZ; Roper Scientific, Göttingen, Germany). These were used to analyze the shape change of the organ as it was deformed by the needle and then released. In these experiments, the needle was placed near the midpoint of the cap cells (Movies S2 and S3). The videos obtained in this case were analyzed by tracking several points along the organ.

Laser ablation

For UV-laser ablation experiments, third-instar larvae expressing a *20xUAS-6xGFP* reporter under the control of the chordotonal neuron driver *iav-GAL4* were used. The lch5 neurons in this line exhibit GFP fluorescence. The animals were heterozygous, and therefore needed to be checked for fluorescence before use. For some of the experiments we used *Sqh-GFP* larvae, where nonmuscle myosin is labeled with GFP, and thus fluorescence is seen not in the neurons, but rather in the ligament and cap cells. Before carrying out the experiments, the larvae were squeezed between a glass slide and a coverslip along with some Ringer's solution, such that the gut was removed and the interior of the larva became transparent. This method leaves the chordotonal organs well preserved and clearly visible, albeit not accessible to direct mechanical manipulation.

A spinning disk confocal microscope (CSU-X1; Carl Zeiss) was used to visualize the lch5 organ with a 100× oil objective (NA 1.4, Plan-APOCHROMAT; Carl Zeiss). Some experiments were performed with a 40× oil objective (NA 1.3, EC Plan-NEOFLUAR; Carl Zeiss), to obtain a large enough field of view to image the complete retraction of the cap cells (see Results and Discussion). Ablation was carried out using a 355-nm pulsed YAG UV laser, average power 14 mW (Rapp OptoElectronic, Wedel, Germany) in click-and-fire mode, with 20% intensity and 300 ms pulse duration per click. The energy delivered was ~0.84 mJ/pulse.

In the laser ablation experiments we used fluorescence microscopy, so that only the neurons and the scolopales were visible in the larvae. The laser was focused either just in front of the scolopales at the initial part of the cap cells on the neuronal dendrites between the scolopales and the neuronal somata, or on the ligament cells. The laser was aimed either at one scolopidium at a time (point focus) or at all scolopidia together (line focus). Videos of the recoil of the organ after ablation were recorded with an AxioCam MRm camera (Carl Zeiss) at a rate of 1 fps. UV-cutting experiments were controlled by the software ROE-SysCon-Zen (Rapp OptoElectronic).

RESULTS AND DISCUSSION

Static elastic deformation of the lch5 organ

We first studied the static deformation of the lch5 organ under stretching by a lateral force applied using a tungsten needle controlled by a micromanipulator (Fig. 2; Movies S2 and S3). The needle was placed near the midpoint of the organ, against the cap cells. From video recordings, we tracked the positions of the scolopales and of the two attachment cells to map the motion and deformation of the entire organ. Lateral displacement near the middle of the organ could have different effects on the organ and its embedding structures: if the organ itself were rather rigid to axial stretching, the cuticle could deform, with the attachment cells moving inward to accommodate this deformation. Alternatively, or in addition, the different cells making up the organ could stretch to various degrees, increasing the length of the organ. In all experiments in which we observed the attachment cells, we could not detect

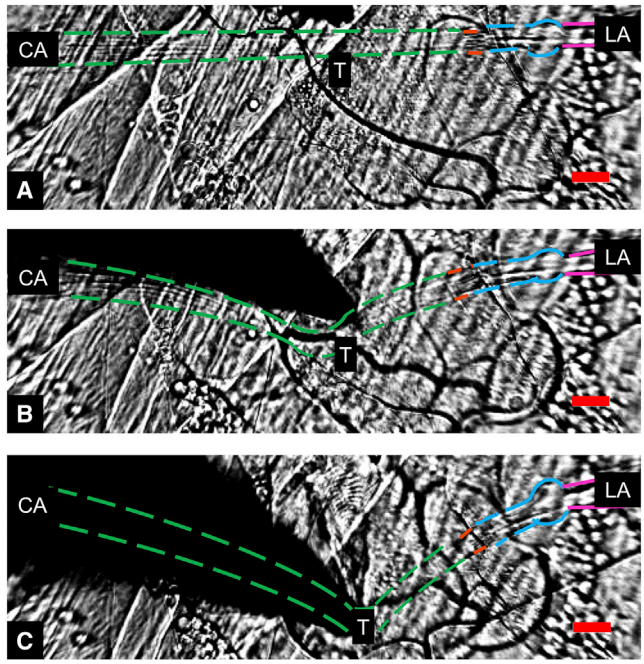

FIGURE 2 Lateral deflection of the lch5 organ. Shown here are (*A*) relaxed, (*B*) weakly deflected (34 μm), and (*C*) strongly deflected (86 μm) configurations. The dark tip is the tungsten needle. The organ is oriented parallel to the long side of the image (neuronal cell bodies on the *right*). Scale bars are 20 μm. Colored dashed lines are the outlines of cells making up the core of the lch5 organ; ligament cells are magenta; neurons with dendrites are blue; scolopales are orange; cap cells are green; point of contact of needle and lch5 organ is T; cap cell attachment cell is CA; and ligament attachment cell is LA. See also Movies S2 and S3. To see this figure in color, go online.

any displacement of the cuticle and the attachment cells when we deformed the lch5 organs (Fig. 2). The organ itself is therefore distinctly more stretch-compliant than the cuticle is to bending and indentation.

The dissection of the larva and the preparation of the fillet lead to some prestrain in the organs that can be estimated from the geometry of the situation. If we consider a third-instar larva as a cylinder of ~1 mm diameter, given that the lch5 organ is ~400 μm long in the fillet, we estimate ~3% increase in the length of the lch5 organ from the intact larva to the fillet.

When the lch5 organ was displaced by the tungsten needle, we measured a substantial, ~10% increase in the length of the organ (from ~320 to ~350 μm for a lateral deflection of 80 μm). This stretch was reversible, and the organs relaxed back to their original lengths when the needle was released (Figs. 2 and 3). The length increase was almost entirely confined to the cap cells. This is demonstrated by tracking four points: the end points of the ligament (LA) and the cap cells (CA); the point of contact of the needle with the lch5 organ (T); and the position of the scolopales (S). We define the axis of the chordotonal organ—the line from CA to LA—as the x axis (Fig. 2). The portion from S to CA corresponds to the cap cells. The length from CA to LA ranged between 300 and 400 μm. The portion between LA and S, i.e., the part of the organ consisting of the ligaments, neuronal somata, dendrites, and scolopales, had a length between 90 and 100 μm before lateral deflection. We observed that during stretches, LA and CA remained fixed (no detectable movement along the x or y axes), whereas T moved along a straight line parallel to the y axis, further away from the position of rest. The length from LA to S also slightly increased, but much less than the length of the cap cells. The cap cells reportedly contain more myosin motors and actin filaments than the sensory neurons, and the scolopales lack myosin while actin is present (35–37). Myosins interacting with actin filaments might provide a mechanism to tense the cap cells and to create stretch elasticity to allow for substantial elongation and subsequent recovery. The observation that the largest part of the elastic strain in the stretched organ occurs in the cap cells implies that they might play an important role in the stretch-sensing mechanism and might be in charge of setting the prestrain and providing adaptation. The dynamics of the normalized strain of the lch5 organ as a function of the relative lateral displacement (absolute displacement divided by the length of the lch5 organ), followed the same curve for several organs from different larvae. Fig. 3 *B* depicts this for four different lch5 organs from four different animals. This shows that the mechanical properties of the lch5 organ are stereotypical and that the dissection process does not appear to alter these dynamics in uncontrolled ways.

The shape of the deformed organ allows us to draw qualitative conclusions about the elastic properties of the organ and of the embedding tissue. In the most stretched conformations, the lch5 organ assumed a concave cusplike shape in the cases where the muscle layers were not removed (Fig. 2, *B* and *C*). This implies that the bending stiffness of the organ is low compared to the stretching stiffness. The shape of the organ would be convex if resistance to bending was dominant. Furthermore, the fact that we observe concave rather than straight shapes points to some coupling to the elastic embedding tissue layers (38).

Relaxation dynamics of the intact lch5 organ

Next, we observed the relaxation dynamics of the deformed organ (Figs. 4 and S2; Movie S4). We again displaced the

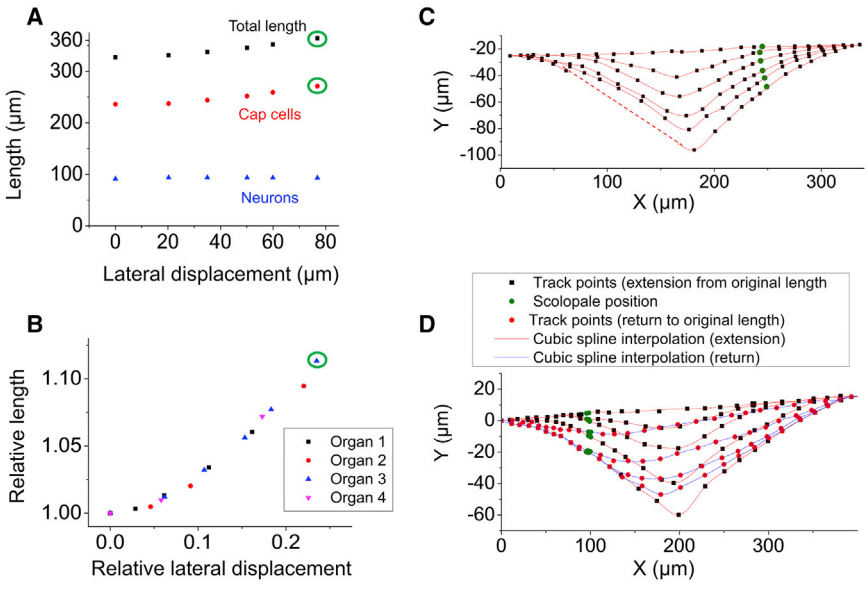

FIGURE 3 Static elastic deformation of the lch5 organ. (*A*) Increase of total length with lateral deflection, entire organ (*black squares*), cap cells (*red circles*), and neuronal part (*blue triangles*). (*B*) Relative increase in length versus relative lateral deflection amplitude for four different lch5 organs, each from a different larva. (*C*) Shapes of a representative lch5 organ (same as Fig. 2) traced from a video recording while the organ was increasingly deflected. (*D*) Shapes of another representative lch5 organ traced from a video recording while the organ was increasingly deflected (*black squares* and *red cubic spline interpolation line*) and during relaxation (*red circles* and *blue cubic spline interpolation line*). See also Movies S2 and S3. In (*C*), part of the last curve has been shown as a dotted line, because this part of the organ was obscured by the needle in the frame of the video corresponding to this curve. The last points in (*A*) and (*B*) are encircled in green for the same reason, and represent a lower bound for the value of the length of the organ at that point. To see this figure in color, go online.

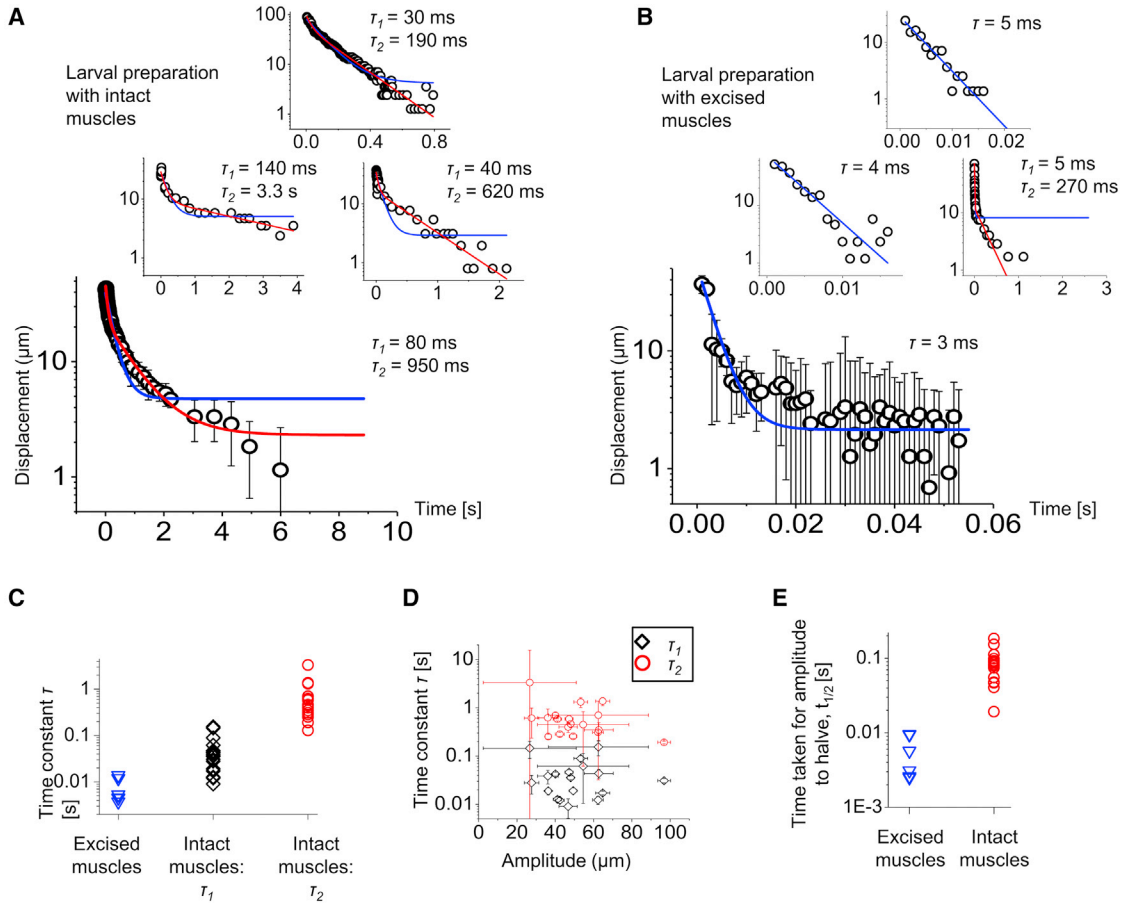

FIGURE 4 Relaxation dynamics of the lch5 organ. (*A*) Relaxation of the midpoint of the organ after lateral deflection and release with intact muscle layers. Each curve is for a different organ in a different animal. Red lines are double-exponential fits with the two time constants τ_1 and τ_2 given. Blue curves represent single-exponential fits. (*B*) Relaxation of the midpoint of the organ after lateral deflection and release with excised muscle layers. Blue lines are single-exponential fits with the time constants τ given. The bottom and middle-left plots are for the same lch5 organ from one larva, and the top and middle-right plots are for the same lch5 organ from a different animal. Except for the middle-right plot, the double-exponential fit has not been shown, because the fit did not converge owing to correlation between the parameters. (*C*) Relaxation time constants of lch5 organs with the covering muscles excised (*blue triangles*), and for lch5 organs covered by intact muscles, τ_1 (*black carets*) and τ_2 (*red circles*). Preparations with intact muscles: four animals were studied. A total of five lch5 organs were investigated. Animal #1: 1 organ, 2 repeats. Animal #2: 2 organs, 3 repeats each. Animal #3: 1 organ, 5 repeats. Animal #4: 1 organ, 5 repeats. Preparations with excised muscles: two organs were studied, each from a different animal, with three repeats per organ. For more details, refer to Figs. S1–S6; Tables S1 and S2. (*D*) Amplitude dependence of lch5 relaxation time constants with muscle layers intact (same experiments as the *black* and *red plots* in (*C*). For more details, refer to Fig. S6). (*E*) Distribution of $t_{1/2}$ values (time taken for the amplitude to reduce to half of its initial value as obtained from the fit) for the experiments with excised muscles, and those with intact muscles. The maximum SD of the error in the data points in (*A* and *B*) was ~6 μm. To see this figure in color, go online.

lch5 organ perpendicular to its long axis with a tungsten needle placed against the cap cells adjacent to the scolopales. We then rapidly released the needle and tracked the relaxation of the organ to its original straight shape. In fillet preparations with the muscle layers above the organ left intact, we observed an initial rapid snap-back after retraction of the needle, followed by a slow relaxation back to a straight conformation (Fig. 4 *A*). The displacement time course was well fitted by a double exponential, which was verified by comparing a double-exponential fit with a single-exponential fit using a reduced χ^2-test. In all cases, the reduced χ^2-value for the double exponential was lower, indicating that this was the better fit (Table S1). The two time constants obtained from this fit, τ_1 and τ_2, ranged from 10 to 150 ms for the initial fast relaxation, and 100 ms to 3 s for the slow relaxation (Fig. 4 *C*). In fillet preparations with the muscles excised, in contrast, a single exponential was sufficient to fit the data because only a rapid snap-back was observed that was faster than in the preparations with intact muscles (Fig. 4 *B*; Table S2). The time constants obtained in this case were approximately an order-of-magnitude smaller than the τ_1-values for the fillets with intact muscles, and ranged from 3 to 15 ms (Fig. 4 *C*). The χ^2-values for the single-exponential fit were smaller than those for the double-exponential fit in two trials in the second organ. In the first organ, two trials showed a lower χ^2-value

for the double-exponential fit. We additionally determined the time $t_{1/2}$, taken for the amplitude of displacement to relax to half its initial value. The values for the experiments with excised muscles ranged from 2 to 10 ms, and for the experiments with intact muscles, they ranged from 19 to 190 ms (Fig. 4 *E*). There was a clear difference of approximately an order of magnitude between the two sets of values.

The lch5 organs are embedded between muscle layers and the cuticle, and bathed in hemolymph. In this situation, a rather high stretch stiffness would be needed to produce an underdamped or oscillatory response, as had been speculated in the literature (39–41). Although the lateral deformation that we applied with the tungsten needles is arguably nonphysiological, it is likely that the viscous damping in the system is similar to what occurs when muscles deform the cuticle and stretch the organ axially. The fact that we observe exponential relaxation and no sign of oscillatory response thus argues for overdamped dynamics. In contrast to a resonant response, an overdamped response makes the organ sensitive to perturbations over a broad frequency range, rather than only near a well-defined resonance frequency.

Most biological materials show a strongly nonlinear elastic response (42,43). To probe for nonlinear response of the lch5 organs, we analyzed the dependence of the relaxation times on the amplitude of the lateral displacement. Within the margins of experimental error, we could not observe an amplitude dependence of these time constants (Fig. 4 *D*). This means that nonlinearities are not strong enough to show significant effects, even at strains of ~20%. This is large compared to the strain for which actin filaments in typical cortical cytoskeletal networks become nonlinear (~5%) (44) and might reflect a geometry of the elastic elements in the cap cells that is optimized for a broad linear response range.

Because the muscle tissue is arranged in layers above the lch5 organ, it might be possible that at least the outermost muscle layer (the lateral muscles) could directly attach to and activate the lch5 organs. This possibility is already discounted in the literature (45,46), but we nevertheless displaced the muscles with the tungsten needle to see if there was any direct coupling between muscle and lch5 displacements (Movie S1). We could not discern any movement of the lch5 organ that would suggest direct elastic coupling to the movement of the muscles. Our data suggest, however, that there is a viscous coupling between the musculature and the lch5 organ, given that the relaxation dynamics are markedly slower in the presence of muscles than those of the bared lch5 organs.

In the relaxation and shape dynamics experiments, the micromanipulator was controlled manually using hydraulic precision actuators. In the relaxation experiments, we placed the needle close to the scolopales; and in the shape dynamics experiments, we placed the needle roughly at the midpoint of the cap cells. We did not aim to measure the precise neuronal responses to small localized tension changes. Instead, our objective was to measure the mechanical response of the whole organ to relatively large displacements. Also, we do not have a priori knowledge of the tension properties of the lch5 organ. Due to this, we concluded that the exact placement of the tungsten needle is not vital to our experiments. Indeed, the relaxation curves we observed were quite reproducible, from which we inferred that the placement of the needle did not have a direct effect on the relaxation. We recorded the videos of the relaxation experiments using bright-field illumination, and tracked them manually using the scolopales as a marker. Similar videos recorded using fluorescence imaging were not usable due to photobleaching. However, because the scolopales are conspicuously visible, the bright-field tracking method was sufficient for our purposes.

Relaxation of the lch5 organ after laser ablation

The straight conformation of the lch5 organ, appearing like a bundle of tense chords (which also inspired the name "chordotonal organs" (39–41)), suggests that there is substantial axial pretension in the cells making up the organ. Tension is balanced along the whole organ, but the ensuing elastic strain might be different for the different cell types. To characterize the prestrain in the different components of intact lch5 organs, we used a UV laser to cut the organ in different planes—through the cap cells near the scolopales (Figs. 5 *A* and 6), through the ligament cells (Fig. 5 *B*), and through the dendrites (Fig. 5 *C*). The response of the organ was observed via the displacement of the GFP-expressing neurons in a fluorescence microscope.

First, we cut the cap cells one by one, by slowly moving the laser focus across the organ (Fig. 6; Movies S5, S6, S7, S8, S9, S10, S11, S12, S13, and S14). When a cap cell was severed, the dendrite belonging to the same scolopidium retracted toward the neuronal somata, and a kink formed where the dendrite enters the scolopale (Fig. 6; Movies S5, S6, S7, S8, S9, S10, S11, S12, S13, and S14). With each cap cell cut, the dendrites collectively retracted further. When the cap cells were completely severed, the scolopales and neuronal dendrites retracted by ~6–15 μm (Figs. 5 *A* and 6, *A* and *D*; Movies S5, S6, S7, S8, S9, S10, S11, S12, S13 and S14; Table S3). Given that the entire lch5 organ is ~400 μm long, and the neuronal part occupies ~80–100 μm of this length, this indicates that, in the intact functional organ, there is a prestrain of ~5–20% in this section. The neuronal somata themselves were not noticeably displaced, which indicates that the axons stably anchor the somata in the surrounding tissue.

When, in the second group of cutting experiments, the dendrites were severed (Fig. 5 *B*; Movies S15, S16, S17, S18, S19, S20, S21, and S22), we could observe the

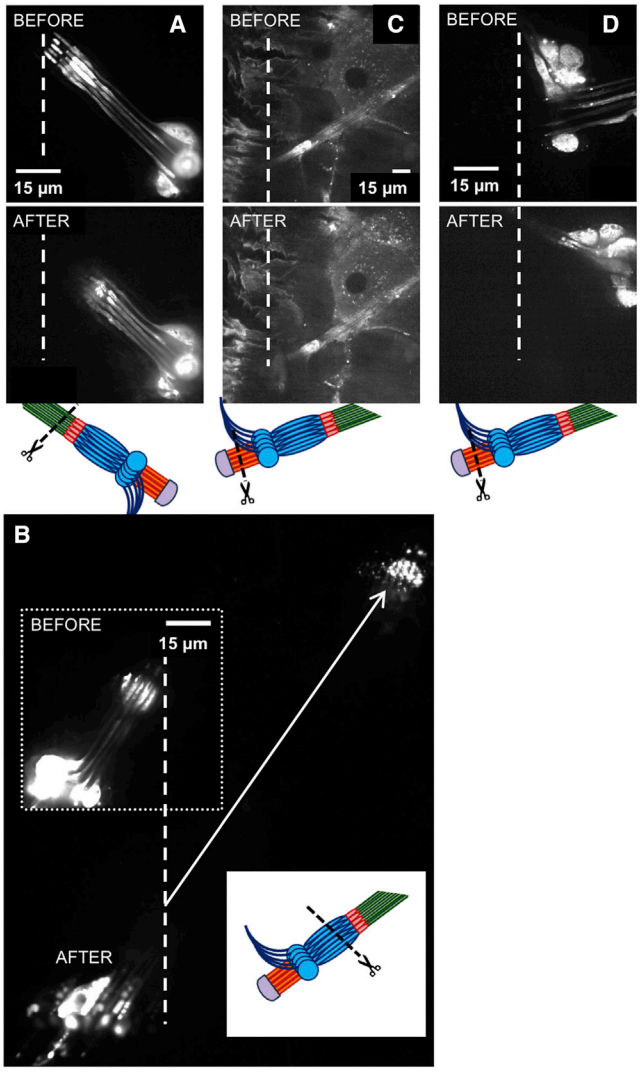

FIGURE 5 Prestrain in the lch5 organ probed by laser ablation. All experiments were done in *iav-Gal4 > 20xUAS-6xGFP* larvae unless mentioned otherwise. The schematics under the subfigures indicate the geometry of laser cutting. Cap cells are not visible, because the animals expressed GFP only in the neuronal part of the lch5 organs. (*A*) Cap cells were severed near the scolopales. The cap cells are again not visible because they were not fluorescent, but their positions are known because they extend straight from the scolopales (Movies S5, S6, S7, S8, S9, S10, S11, S12, S13, and S14). (*B*) Dendrites of the neurons were severed between somata and scolopales. The vertical dotted line shows the position of the scolopales before ablation, and the diagonal arrow pointing toward the top right indicates their new position after they had retracted by ~100 μm (Movies S15, S16, S17, S18, S19, S20, S21, and S22). (*C*) Ligament cells were cut whereas the cap cells are still intact. There is a small retraction, but no other change in the lch5 organ. The fly line used for this was *Sqh-GFP*, where the ligaments and cap cells are fluorescent due to labeling of myosin, but not the neurons (Movie S23). (*D*) Ligament cells were cut after severing the cap cells. Some retraction is seen (Movie S24). Scale bars, 15 μm. To see this figure in color, go online.

relaxation of both sides of the organ by following the retracting fluorescent neuronal somata toward the ligament cell side and the retracting fluorescent dendritic fragments toward the cap cell side. We performed two types of cutting experiments in this location, cutting the dendrites all at once (e.g., Movie S15), or one by one (e.g., Movie S17). Either way, when the dendrites were all cut, the severed dendritic fragments, and the scolopales along with the cap cells, retracted rapidly by ~100 μm. Given that the cap cells are 200–300 μm long, this corresponds to a prestrain of ~30–50% in this section of the lch5 organ (Table S3).

In the third set of experiments, we severed the ligament cells. When the ligament cells were severed with the cap cells intact, the neuronal somata were still anchored by their axons, and moved in the direction of the cap cells by only ~7 μm (Fig. 5 *C*; Movie S23). When the axons were then also severed, however, the neuronal somata along with the dendrites and scolopales rapidly retracted in the direction of the cap cells, to a similar extent as seen in the second set of experiments (Movie S25). When in one control experiment we severed the ligament cells after cutting the cap cells, we observed a slow drift of the neuronal somata toward the cap cells by ~30 μm (Fig. 5 *D*; Movie S24).

These results point to a role of the cap cells as the dominant elastic elements in the lch5 organs, consistent with what we found when we overstretched the organ by lateral deflection, where the additional strain was again mostly localized to the cap cells. Because the cap cells also contain substantial amounts of myosin and actin, it is intriguing to speculate that these cells build up—and regulate—organ tension.

CONCLUSIONS

We found that the lch5 organs of *Drosophila* larvae show remarkable stretch elasticity with a large linear range. When stretched and released, they relax in an overdamped fashion, viscously, but not elastically coupled to overlying muscle layers. Upon laser cutting, the organ recoils with a large amplitude, which demonstrates a large prestrain of up to 50% in the cap cells of the functioning organ. It will be interesting to explore the role of this prestrain and the associated pretension and its regulation in the sensing mechanism of lch5 chordotonal organs. We anticipate that this tension is actively regulated and that it facilitates mechanotransduction in chordotonal sensory neurons, e.g., by maximizing the sensitivity of mechanotransduction channels through keeping their open probability at rest at its half-maximum value, where small mechanical stimuli would cause the maximal open probability change. A half-maximum open probability at rest had been reported for mechanotransduction channels in the chordotonal organs within Johnston's organ of adult flies (13), where, analogous to vertebrate hair cells (23), adaptation motors in the sensory cells appear to stabilize the resting open probability of the channels (13,28). The latter adaptation is fast with time constants between 4 and 12 ms (13). If we assume that the

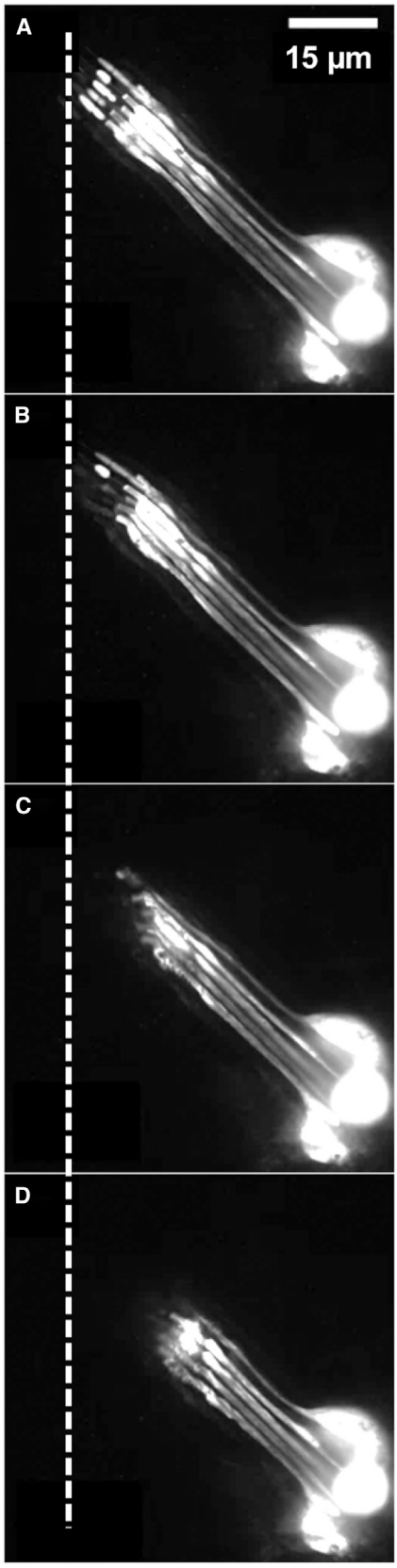

FIGURE 6 Relaxation of lch5 organ during sequential severing of cap cells by laser ablation near the scolopales (see Fig. 4 *A*; Movie S5). Only the neurons expressed GFP. (*A*) Shown before ablation. (*B–D*) Shown here is the retraction of the neuronal dendrites as the cap cells were severed one by one: (*B*) after severing one cap cell from the bottom; (*C*) after severing three cap cells from the bottom; and (*D*) after severing all five cap cells.

fast relaxation process we observed in the larval organs is related to adaptation, it seems that a much slower adaptation mechanism might reside in the supporting cap cells that regulates the resting tension in these sensory cells. This slow adaptation mechanism might co-occur with a fast adaptation mechanism in lch5 neurons, which not only monitor slow body movements but reportedly show adapting spiking responses to sound-induced substrate vibrations at frequencies of several 100 Hz (32,47). Future work will have to address the molecular details of both sensory transduction and tension regulation in lch5 as well as target the intriguing question of how a signal in one cell, the sensory neuron, can connect to tension-generating machinery in another cell, the cap cell.

SUPPORTING MATERIAL

Seven figures, three tables, and twenty-five movies are available at http://www.biophysj.org/biophysj/supplemental/S0006-3495(17)31144-X.

AUTHOR CONTRIBUTIONS

C.F.S. and M.C.G. designed the research. A.P. performed the research. C.S. provided support with basic *Drosophila* experimental know-how. D.K. and J.G. provided support with the UV cutting experiments. A.P. and C.F.S. analyzed data. A.P., M.C.G., and C.F.S. wrote the article.

ACKNOWLEDGMENTS

We thank Ben Warren and Chonglin Guan for helping with the experiments and Bart Geurten for providing an electrolytic sharpening device.

This research was supported by the Bernstein Center for Computational Neuroscience Göttingen (BCCN) (to M.C.G. and C.F.S.), the Deutsche Forschungsgemeinschaft (DFG) Cluster of Excellence Research Center "Nanoscale Microscopy and Molecular Physiology of the Brain (CNMPB)" (to C.F.S.), and Collaborative Research Centers (SFB) SFB 937, A10 (to J.G. and C.F.S.) and SFB 889, A1 (to M.C.G.).

REFERENCES

1. Aiello, B. R., M. W. Westneat, and M. E. Hale. 2017. Mechanosensation is evolutionarily tuned to locomotor mechanics. *Proc. Natl. Acad. Sci. USA.* 114:4459–4464.
2. Heckscher, E. S., S. R. Lockery, and C. Q. Doe. 2012. Characterization of *Drosophila* larval crawling at the level of organism, segment, and somatic body wall musculature. *J. Neurosci.* 32:12460–12471.
3. Field, L. H., and T. Matheson. 1998. Chordotonal organs of insects. *Adv. Insect Physiol.* 27:1–228.
4. Kamikouchi, A., H. K. Inagaki, …, K. Ito. 2009. The neural basis of *Drosophila* gravity-sensing and hearing. *Nature.* 458:165–171.
5. Göpfert, M. C., and R. M. Hennig. 2016. Hearing in insects. *Annu. Rev. Entomol.* 61:257–276.

6. Yorozu, S., A. Wong, …, D. J. Anderson. 2009. Distinct sensory representations of wind and near-field sound in the *Drosophila* brain. *Nature*. 458:201–205.
7. Fuller, S. B., A. D. Straw, …, M. H. Dickinson. 2014. Flying *Drosophila* stabilize their vision-based velocity controller by sensing wind with their antennae. *Proc. Natl. Acad. Sci. USA*. 111:E1182–E1191.
8. Sun, Y., L. Liu, …, M. J. Welsh. 2009. TRPA channels distinguish gravity sensing from hearing in Johnston's organ. *Proc. Natl. Acad. Sci. USA*. 106:13606–13611.
9. Yack, J. E. 2004. The structure and function of auditory chordotonal organs in insects. *Microsc. Res. Tech.* 63:315–337.
10. Halachmi, N., A. Nachman, and A. Salzberg. 2012. Visualization of proprioceptors in *Drosophila* larvae and pupae. *J. Vis. Exp*. 2012 Jun 13;(64):e3846. https://doi.org/10.3791/3846.
11. Hertweck, H. 1931. Anatomie und Variabilität des Nervensystems und der Sinnesorgane von *Drosophila melanogaster* (Meigen). University of Frankfurt, Akademische Verlagsgesellschaft m. b. H., Leipzig, Germany.
12. Senthilan, P. R., D. Piepenbrock, …, M. C. Göpfert. 2012. *Drosophila* auditory organ genes and genetic hearing defects. *Cell.* 150:1042–1054.
13. Nadrowski, B., J. T. Albert, and M. C. Göpfert. 2008. Transducer-based force generation explains active process in *Drosophila* hearing. *Curr. Biol.* 18:1365–1372.
14. Göpfert, M. C., and D. Robert. 2002. The mechanical basis of *Drosophila* audition. *J. Exp. Biol.* 205:1199–1208.
15. Göpfert, M. C., J. T. Albert, …, A. Kamikouchi. 2006. Specification of auditory sensitivity by *Drosophila* TRP channels. *Nat. Neurosci.* 9:999–1000.
16. Effertz, T., R. Wiek, and M. C. Göpfert. 2011. NompC TRP channel is essential for *Drosophila* sound receptor function. *Curr. Biol.* 21:592–597.
17. Albert, J. T., B. Nadrowski, and M. C. Göpfert. 2007. Mechanical signatures of transducer gating in the *Drosophila* ear. *Curr. Biol.* 17:1000–1006.
18. Martinac, B., and C. D. Cox. 2016. Mechanosensory transduction: focus on ion channels. *In* Comprehensive Biophysics. Elsevier, Amsterdam, the Netherlands.
19. Yan, Z., W. Zhang, …, Y. N. Jan. 2013. Drosophila NOMPC is a mechanotransduction channel subunit for gentle touch sensation. *Nature.* 493:221–225.
20. Christensen, A. P., and D. P. Corey. 2007. TRP channels in mechanosensation: direct or indirect activation? *Nat. Rev. Neurosci.* 8:510–521.
21. Zanini, D., and M. C. Göpfert. 2013. Mechanosensation: tethered ion channels. *Curr. Biol.* 23:R349–R351.
22. Hudspeth, A. J. 2008. Making an effort to listen: mechanical amplification in the ear. *Neuron.* 59:530–545.
23. Hudspeth, A. J., Y. Choe, …, P. Martin. 2000. Putting ion channels to work: mechanoelectrical transduction, adaptation, and amplification by hair cells. *Proc. Natl. Acad. Sci. USA*. 97:11765–11772.
24. Martin, P., and A. J. Hudspeth. 1999. Active hair-bundle movements can amplify a hair cell's response to oscillatory mechanical stimuli. *Proc. Natl. Acad. Sci. USA*. 96:14306–14311.
25. Martin, P., and A. J. Hudspeth. 2001. Compressive nonlinearity in the hair bundle's active response to mechanical stimulation. *Proc. Natl. Acad. Sci. USA*. 98:14386–14391.
26. Martin, P., A. J. Hudspeth, and F. Jülicher. 2001. Comparison of a hair bundle's spontaneous oscillations with its response to mechanical stimulation reveals the underlying active process. *Proc. Natl. Acad. Sci. USA*. 98:14380–14385.
27. Göpfert, M. C., and D. Robert. 2003. Motion generation by *Drosophila* mechanosensory neurons. *Proc. Natl. Acad. Sci. USA*. 100:5514–5519.
28. Karak, S., J. S. Jacobs, …, M. C. Göpfert. 2015. Diverse roles of axonemal dyneins in *Drosophila* auditory neuron function and mechanical amplification in hearing. *Sci. Rep.* 5:17085.
29. DiCaprio, R. A., H. Wolf, and A. Büschges. 2002. Activity-dependent sensitivity of proprioceptive sensory neurons in the stick insect femoral chordotonal organ. *J. Neurophysiol.* 88:2387–2398.
30. Rydqvist, B., N. Purali, and J. Lännergren. 1994. Visco-elastic properties of the rapidly adapting stretch receptor muscle of the crayfish. *Acta Physiol. Scand.* 150:151–159.
31. Caldwell, J. C., M. M. Miller, …, D. F. Eberl. 2003. Dynamic analysis of larval locomotion in *Drosophila* chordotonal organ mutants. *Proc. Natl. Acad. Sci. USA*. 100:16053–16058.
32. Zhang, W., Z. Yan, …, Y. N. Jan. 2013. Sound response mediated by the TRP channels NOMPC, NANCHUNG, and INACTIVE in chordotonal organs of *Drosophila* larvae. *Proc. Natl. Acad. Sci. USA*. 110:13612–13617.
33. Marley, R., and R. A. Baines. 2011. Dissection of first- and second-instar *Drosophila* larvae for electrophysiological recording from neurons: the flat (or fillet) preparation. *Cold Spring Harb. Protoc.* 2011:pdb.prot065649.
34. http://www.digitaladdis.com/sk/PDMS_Mold_Preparation_Kassegne_MEMSLab.pdf.
35. Wolfrum, U. 1997. Cytoskeletal elements in insect sensilla. *Int. J. Insect Morphol. Embryol.* 26:191–203.
36. Wolfrum, U. 1990. Actin-filaments—the main components of the scolopale in insect sensilla. *Cell Tiss. Res.* 261:85–96.
37. Wolfrum, U. 1992. Cytoskeletal elements in ciliary receptor systems. *Cell Motil. Cytoskeleton.* 23:311.
38. Brangwynne, C. P., F. C. MacKintosh, …, D. A. Weitz. 2006. Microtubules can bear enhanced compressive loads in living cells because of lateral reinforcement. *J. Cell Biol.* 173:733–741.
39. Wheeler, W. M. 1965. Ants: Their Structure, Development and Behavior.. Columbia University Press, New York, NY.
40. Graber, V. 1881. Die chordotonalen sinnesorgane und das gehör der insecten. *Archiv für M*ikroskopische Anatomie. 20:506–640.
41. von Siebold, C. T. 1844. Über das stimm—und gehörorgan der orthopteren. *Arch. für Naturgesch.* 10:52–81.
42. Storm, C., J. J. Pastore, …, P. A. Janmey. 2005. Nonlinear elasticity in biological gels. *Nature.* 435:191–194.
43. Carrillo, J. M. Y., F. C. MacKintosh, and A. V. Dobrynin. 2013. Nonlinear elasticity: from single chain to networks and gels. *Macromolecules.* 46:3679–3692.
44. Janmey, P. A., S. Hvidt, …, T. P. Stossel. 1994. The mechanical properties of actin gels. Elastic modulus and filament motions. *J. Biol. Chem.* 269:32503–32513.
45. Halachmi, N., A. Nachman, and A. Salzberg. 2016. A newly identified type of attachment cell is critical for normal patterning of chordotonal neurons. *Dev. Biol.* 411:61–71.
46. Klein, Y., N. Halachmi, …, A. Salzberg. 2010. The proprioceptive and contractile systems in *Drosophila* are both patterned by the EGR family transcription factor Stripe. *Dev. Biol.* 337:458–470.
47. Scholz, N., J. Gehring, …, T. Langenhan. 2015. The adhesion GPCR latrophilin/CIRL shapes mechanosensation. *Cell Reports.* 11:866–874.

Biophysical Journal, Volume *113*

Supplemental Information

Mechanical Properties of a *Drosophila* Larval Chordotonal Organ

Achintya Prahlad, Christian Spalthoff, Deqing Kong, Jörg Großhans, Martin C. Göpfert, and Christoph F. Schmidt

Supplementary Figures and Tables

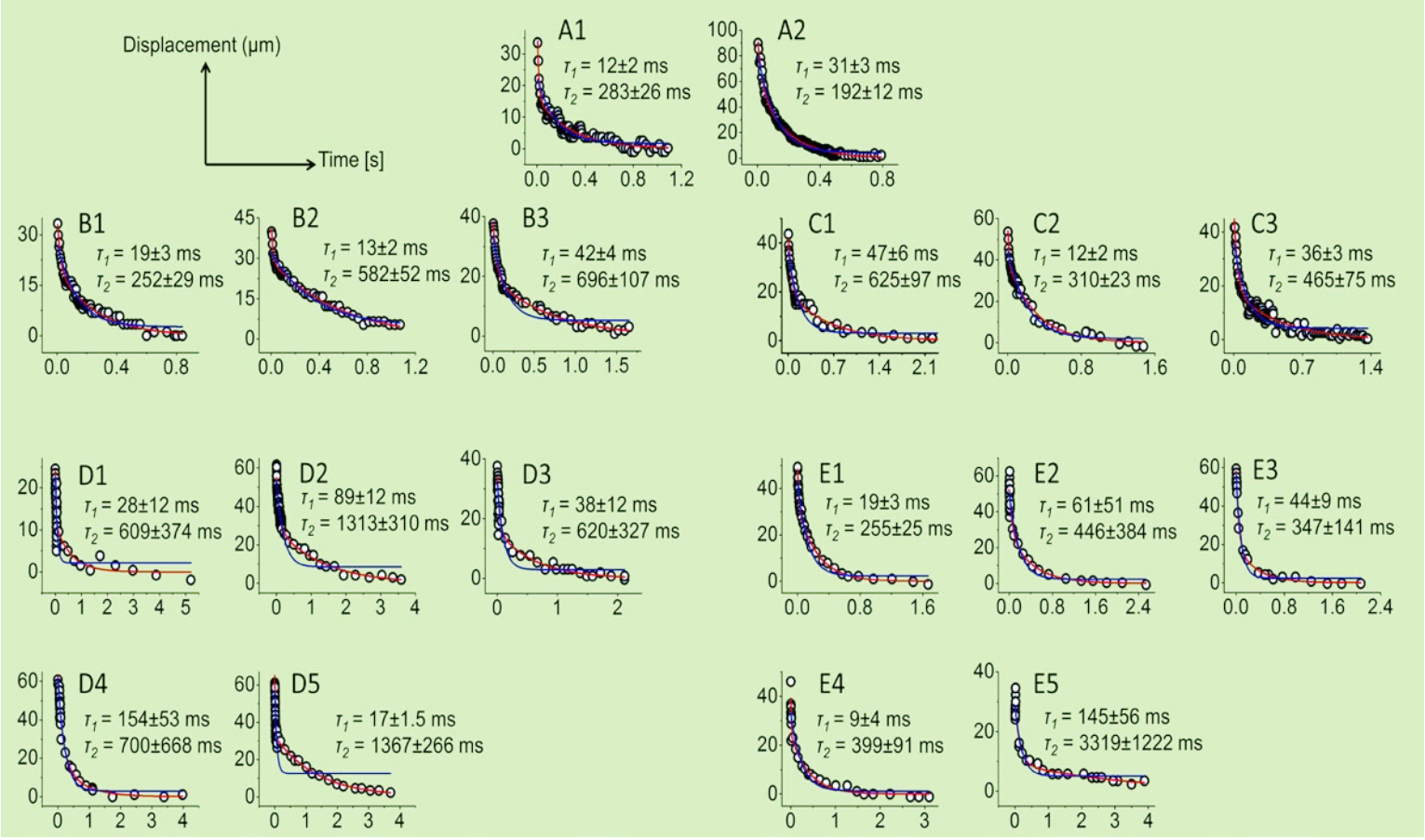

Fig. S1. Relaxation curves of laterally deflected lch5 organs for all the relaxation experiments in larval preparations with intact muscles, showing double-exponential fits (red curves) and single-exponential fits (grey curves). Reduced χ^2 values for single- and double-exponential fits are given in Table S1.

The maximum standard deviation of the error in the data points was approx. 6 µm.

A1, A2: Animal 1, lch5 organ 1
B1, B2, B3: Animal 2, lch5 organ 1
C1, C2, C3: Animal 2, lch5 organ 2
D1-D5: Animal 3, lch5 organ 1
E1-E5: Animal 4, lch5 organ 1

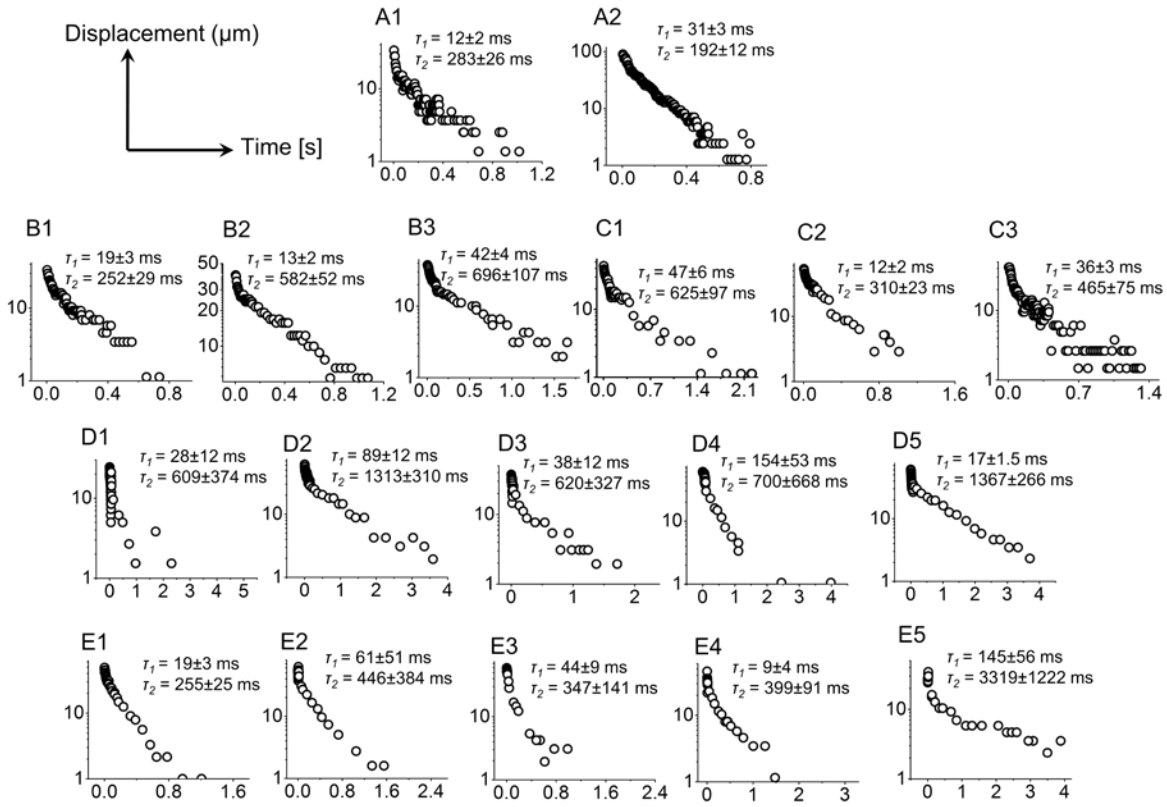

Fig. S2. Relaxation curves of laterally deflected lch5 organs for all the relaxation experiments in larval preparations with intact muscles, with y-axes converted to logarithmic scale. Reduced χ^2 values for single- and double-exponential fits are given in Table S1.

A1, A2: Animal 1, lch5 organ 1
B1, B2, B3: Animal 2, lch5 organ 1
C1, C2, C3: Animal 2, lch5 organ 2
D1-D5: Animal 3, lch5 organ 1
E1-E5: Animal 4, lch5 organ 1

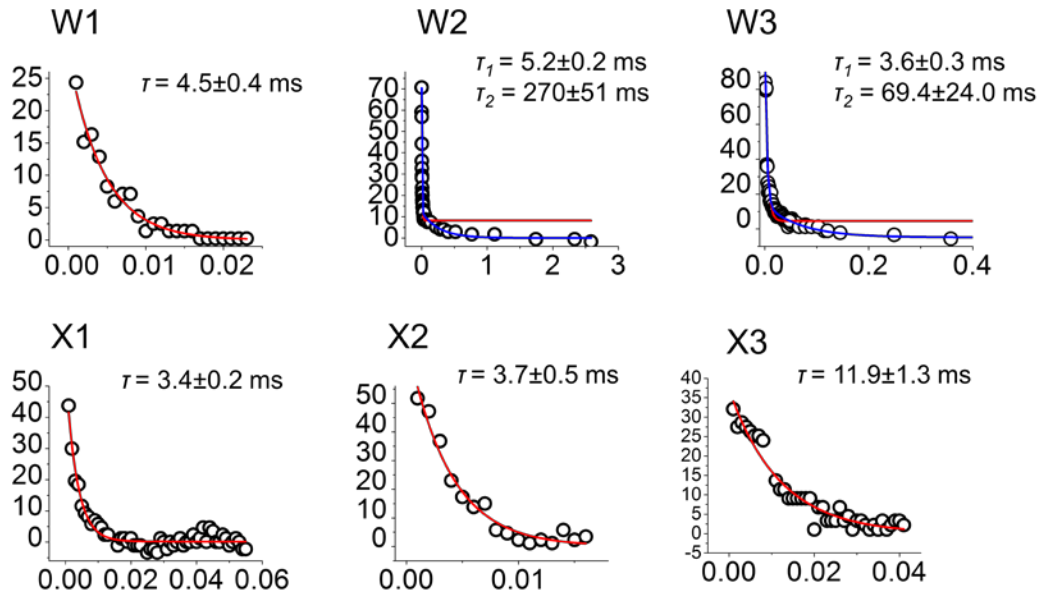

Fig. S3. Relaxation curves of laterally deflected lch5 organs for all the relaxation experiments in larval preparations with excised muscles, showing exponential fits. Red curves represent single exponential fits, and blue curves represent double exponential fits. In the graphs where double exponential fits are not shown, these fits either do not converge, or coincide with the single exponential fits. Reduced χ^2 values for single- and double-exponential fits are given in Table S1.

W1, W2, W3: Animal 1, lch5 organ 1
X1, X2, X3: Animal 2, lch5 organ 2

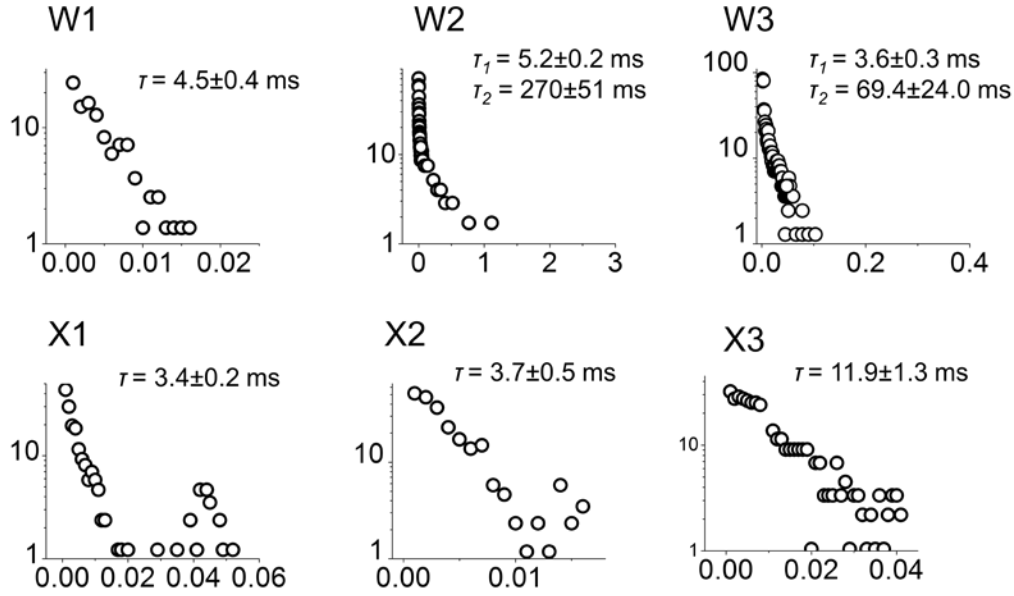

Fig. S4. Relaxation curves of laterally deflected lch5 organs for all the relaxation experiments in larval preparations with excised muscles, with y-axes converted to logarithmic scale. Reduced χ^2 values for single- and double-exponential fits are given in Table S1.

W1, W2, W3: Animal 1, lch5 organ 1
X1, X2, X3: Animal 2, lch5 organ 2

Experimental animal	Ich5 organ	Trial	Reduced χ^2 values	
			Single exponential fit	Double exponential fit
1	A	A1	4.73	1.74
		A2	7.42	2.44
2	B	B1	2.93	1.13
		B2	3.72	0.72
		B3	5.38	0.85
	C	C1	5.84	1.81
		C2	5.51	1.82
		C3	6.14	2.00
3	D	D1	6.62	5.91
		D2	5.89	3.45
		D3	8.53	6.82
		D4	9.14	8.58
		D5	21.38	4.74
4	E	E1	5.94	5.60
		E2	5.27	1.32
		E3	23.40	22.46
		E4	6.15	3.77
		E5	10.60	6.79

Table S1. Exponential fits of the relaxation curves of laterally deflected Ich5 organs. Quality of fit is judged by the χ^2 test. Reduced χ^2 values for double- and single-exponential fits for the data plots from relaxation experiments for Ich5 organs in larval preparations with intact muscles. These values indicate the relative goodness of fit. The model that has a lower χ^2 value is considered as a better fit for the data. The double-exponential model is seen to provide the better fit. In two cases (E1 and E3), the difference in the χ^2 values for single and double exponential fits is small, but nonetheless, the double-exponential model has the lower value.

Experimental animal	lch5 organ	Trial	Reduced χ^2 values	
			Single exponential fit	Double exponential fit
1	W	W1	1.15	1.05
		W2	8.56	1.35
		W3	64.79	66.59
2	X	X1	2.80	2.55
		X2	7.37	8.71
		X3	3.54	3.75

Table S2. Exponential fits of the relaxation curves of laterally deflected lch5 organs. Quality of fit is judge by the χ^2 test. Reduced χ^2 values for double- and single-exponential fits for the data plots from relaxation experiments for lch5 organs in larval preparations with excised muscles. The values indicate the relative goodness of fit. The model that has a lower χ^2 value is considered as a better fit for the data.

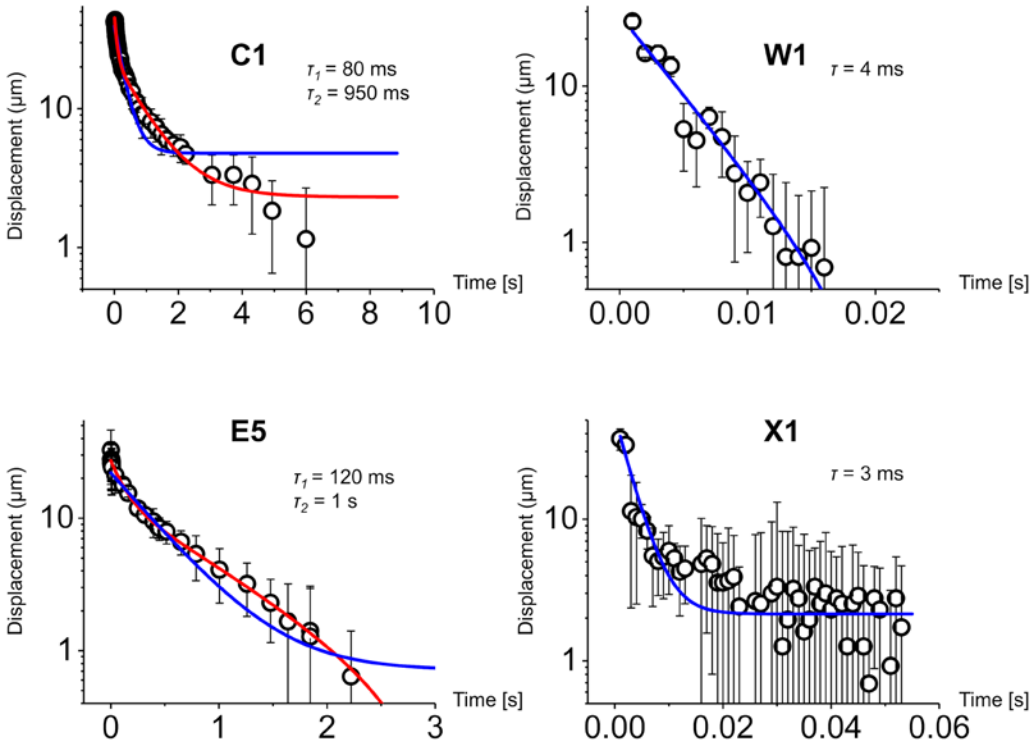

Fig. S5. Error analysis for four experiments: C1, E5 (muscles intact) and W1, X1 (muscles excised). Error bars represent twice the standard deviation of the Y-value.

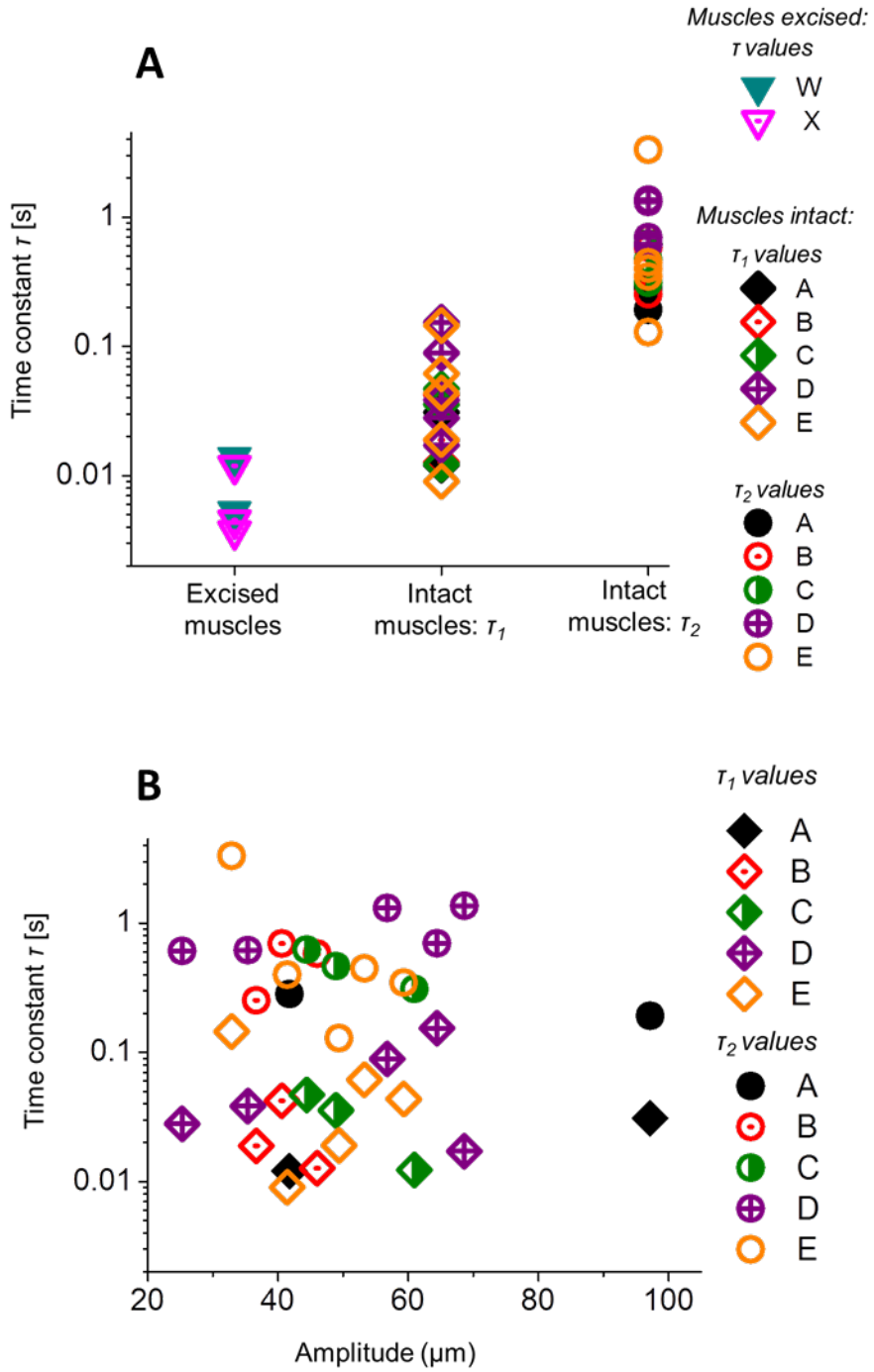

Fig. S6. Time constants for all relaxation experiments. W and X represent the larval preparations with muscles excised (time constants shown as inverted triangles), and A, B, C, D, E refer to the experiments on preparations with intact muscles (see fig. S1 and tables S1 and S2). In this case, diamonds represent the first time constant τ_1 and circles represent the second time constant τ_2. **(A)** Distribution of time constant values (refer to fig. 4C). **(B)** Plot of time constants versus amplitude for the preparations with intact muscles (refer to fig. 4D).

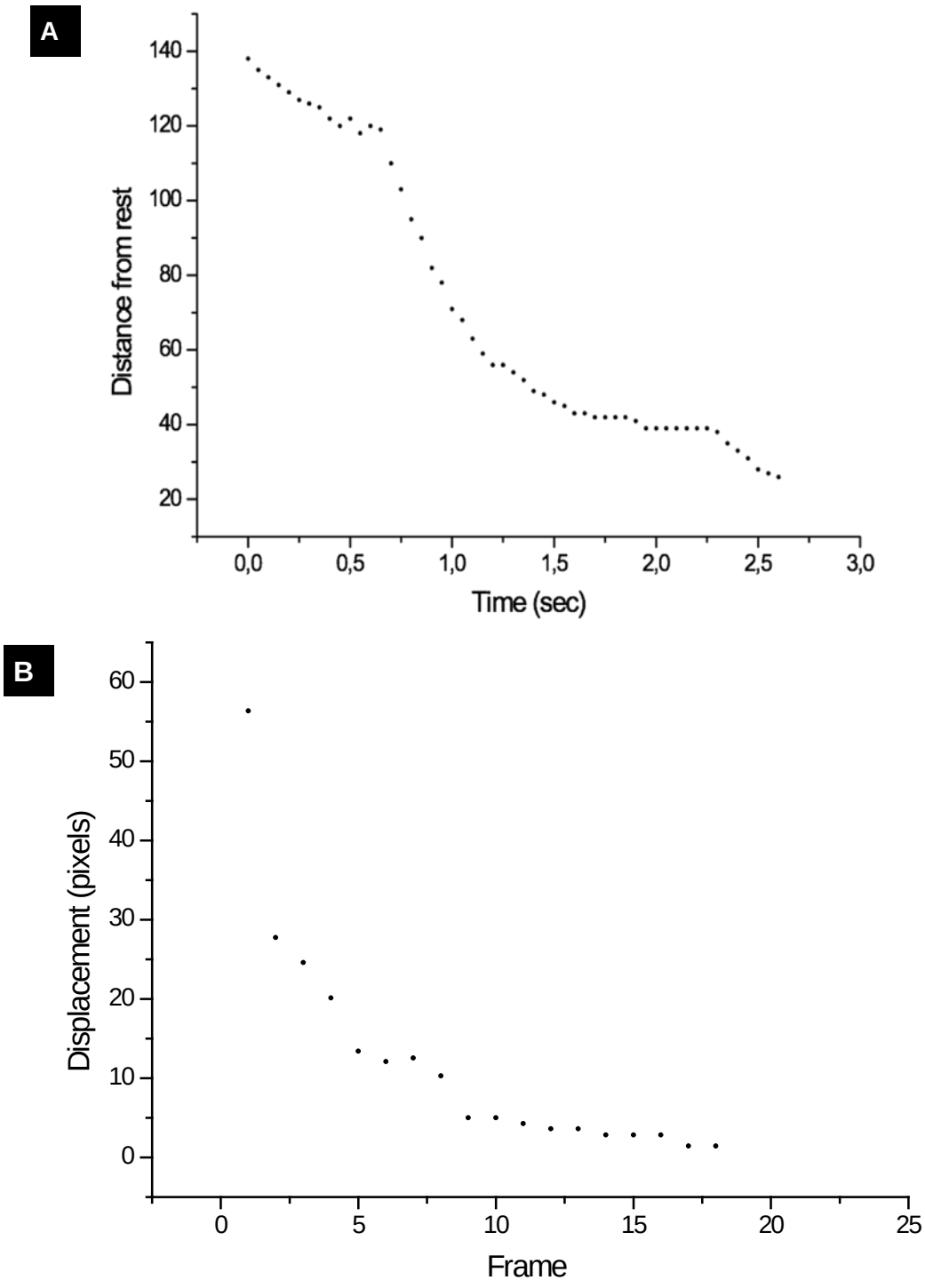

Fig. S7. (A) Incomplete disengagement of the lch5 organ from the tungsten needle, indicated by a plateau in the graph at around 0.5 sec. Displacement values are in pixels. **(B)** Data points missing from the displacement vs time plot, owing to low frame rate of the camera. In this plot, displacement is in pixels, and the X-axis represents the frame number of the video.

Supplementary Movies

Movie S0: Displacement of the muscles by the tungsten needle does not significantly deform the lch5 organ. The tungsten needle enters the sample from the top left corner. Scale bar: 50 µm.

Movie S1, deformation of the lch5 organ during lateral deflection by a tungsten needle: Needle placed near the middle of the organ to analyse the shape of the lch5 organ. Image laterally inverted for convenient viewing in comparison to other images. Arrows indicate the direction in which the scolopales and somata move upon being displaced by the needle. Scale bar: 50 µm.

CA: Cap attachment cell
LA: Ligament attachment cell
sc: Scolopales
n: Neuronal somata

Movie S2, deformation of the lch5 organ during lateral deflection by a tungsten needle: Another example of the same experiment as in M1. Arrows indicate the direction in which the scolopales and somata move upon being displaced by the needle. Scale bar: 50 µm.

CA: Cap attachment cell
LA: Ligament attachment cell
sc: Scolopales
n: Neuronal somata

Movie S3, relaxation of the lch5 organ after lateral deflection by a tungsten needle: Needle placed closer to the scolopales. Arrows indicate the direction in which the scolopales and somata move upon being released from the needle. Scale bar: 50 µm.

CA: Cap attachment cell
LA: Ligament attachment cell
sc: Scolopales
n: Neuronal somata

Movie S4, severing the cap cells: Retraction of dendrites and kink formation at the scolopale-dendrite junction upon severing the cap cells using a laser. The retraction is towards the bottom right. Scale bar: 15 µm.

N: Neuronal somata
Sc: Scolopales
De: Dendrites

Movie S5, severing the cap cells: Same experiment as in Movie S4. The retraction is towards the top left. Scale bar: 15 µm.

N: Neuronal somata
Sc: Scolopales
De: Dendrites

Movie S6, severing the cap cells: Same experiment as in Movie S4. Here only the dendrites and scolopales are visible. The retraction is towards the top left again. Scale bar: 15 μm.

Sc: Scolopales
De: Dendrites

Movie S7, severing the cap cells: Same experiment as in Movie S4. The retraction is towards the top right. Scale bar: 15 μm.

Sc: Scolopales
De: Dendrites

Movies S8-S9, severing the cap cells: Same experiment as in Movie S4. In S8 the dendrites are slightly extended due to application of the laser. In S9 the cap cells are severed, and the dendrites retract. The retraction is towards the bottom left. Scale bar: 15 μm.

N: Neuronal somata
Sc: Scolopales
De: Dendrites

Movie S10, severing the cap cells: Same experiment as in Movie S4. The retraction is towards the bottom left. It is incomplete owing to severing of only 3 cap cells out of 5. Scale bar: 15 μm.

N: Neuronal somata
Sc: Scolopales
De: Dendrites

Movie S11, severing the cap cells: Same experiment as in Movie S4. The retraction is towards the bottom left. Here, the scolopidia are seen to split, with the lower three retracting further than the upper two. This is possibly because the laser was aimed in between two scolopidia. Scale bar: 15 μm.

N: Neuronal somata
Sc: Scolopales
De: Dendrites

Movie S12, severing the cap cells: Same experiment as in Movie S4. The retraction is towards the top right. Scale bar: 15 μm.

N: Neuronal somata
Sc: Scolopales
De: Dendrites

Movie S13, severing the cap cells: Same experiment as in Movie S4. The retraction is towards the left. This video uses bright-field illumination. Scale bar: 15 μm.

N: Neuronal somata
Sc: Scolopales
De: Dendrites

Movies S14-S15, severing the dendrites: UV-Laser cutting of the dendrites leads to rapid retraction of the scolopales attached to the contracting cap cells. The dendrites were cut all at once, under 100X magnification. The scolopales retract towards the top right. Movie S14 depicts the experiment, and Movie S15 (40X magnification) shows the extent of retraction. Scale bar: 15 µm.

N: Neuronal somata
Sc: Scolopales
De: Dendrites

Movies S16-S17, severing the dendrites: Same experiment as in Movies S14-S15, under 40X magnification. The scolopales retract towards the top right. Scale bar: 15 µm.

N: Neuronal somata
Sc: Scolopales
De: Dendrites

Movies S18-S19, severing the dendrites: Same experiment as in Movies S14-S15. Movie S18 was recorded under 100X magnification, and Movie S19 was recorded under 40X magnification. The scolopales retract towards the top left. Scale bar: 15 µm.

N: Neuronal somata
Sc: Scolopales
De: Dendrites

Movie S20, severing the dendrites: Same experiment as in Movies S14-S15. Recorded under 40X magnification. The scolopales retract towards the top left. Scale bar: 15 µm.

N: Neuronal somata
Sc: Scolopales
De: Dendrites

Movie S21, severing the dendrites: Same experiment as in Movies S14-S15. Recorded under 40X magnification. The scolopales retract towards the bottom right. The cap cells are faintly visible and are observed to retract. Scale bar: 15 µm.

Sc: Scolopales
De: Dendrites
C: Cap cells

Movie S22, severing the ligament cells: UV-Laser cutting of the ligament cells subsequent to cutting the cap cells. Axons are still attached to the neuronal cell bodies. The organ retracts slightly to the right. Scale bar: 15 µm.

N: Neuronal somata
Sc: Scolopales
De: Dendrites
L: Ligament
A: Axons

Movie S23, severing the ligament cells: UV-Laser cutting of the ligament cells subsequent to cutting the cap cells. The organ retracts slightly to the right. This was carried out in a Sqh-GFP larva, with fluorescent cap cells and ligament (no fluorescence in the neuronal part). Scale bar: 15 µm.

C: cap cells
De: Dendrites
L: Ligament

Movie S24, severing the ligament cells: UV-Laser cutting of the ligament cells, followed by cutting the axons. When only the ligament cells are severed, there is negligible movement. When then the axons are also severed, the remaining organ retracts strongly and rapidly towards the cap cells. Scale bar: 15 µm.

N: Neuronal somata
Sc: Scolopales
De: Dendrites
L: Ligament
A: Axons

Ablation carried out in	**Movie**	**Retraction observed in**	**Retraction (in µm)**
Cap cells	S4	Dendrites	15
	S5		9
	S6		6
	S7		5
	S8		3 (slight extension)
	S9		10 (retraction)
	S10		6
	S11		15
	S12		8
	S13		9
			Average: 9
Dendrites	S14-S15	Cap cells (indicated by scolopale motion)	120
	S16-S17		134
	S18-S19		62
	S20		81
	S21		62
			Average: 92

Ligament (after ablating axons)	S22	Neurons	28
Ligament	S23	Ligament	7

Table S3. Quantification of the retraction of the lch5 organ observed in the laser ablation videos